A parametrized BVI noise prediction code

G. Reboul

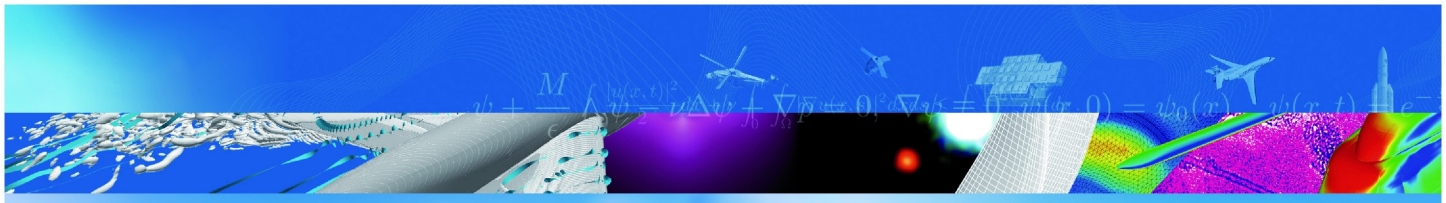

T I R É À P A R T

A parametrized BVI noise prediction code.

G. Reboul

Greener Aviation 2014
BRUXELLES, BELGIQUE
12-14 mars 2014

TP 2014-307

ONERA
THE FRENCH AEROSPACE LAB

retour sur innovation

A parametrized BVI noise prediction code.

Un code paramétrable de prévision du bruit d'interaction pale-tourbillon.

par

G. Reboul

Résumé traduit :

Le code Flap a été développé pour prédire le bruit d'interaction pale-tourbillon à un stade précoce du développement d'un hélicoptère. A cet effet, le code doit posséder un temps d'exécution réduit et nécessiter un faible nombre de données d'entrée. Cet article présente les dernières améliorations qui ont été réalisées dans le cadre du programme CleanSky JTI , dans lequel le code Flap est utilisé pour alimenter une base de données de bruit rayonné sous forme d'hémisphère. Pour chaque hélicoptère, des calculs de référence sont effectuées par le DLR et le CIRA en utilisant des codes possédant un niveau plus élevé de la modélisation que Flap, mais aussi un temps de calcul plus important. Ces calculs sont ensuite utilisés pour étalonner le code Flap qui est ensuite utilisé pour générer les hémisphères restantes. Par conséquent, la généralisation du modèle de sillage est nécessaire pour permettre une bonne calibration. C'est ce qui est présenté dans un premier temps, en plus des autres améliorations effectuées et d'une brève présentation du code. De plus, en ce qui concerne la position radiale de l'enroulement tourbillonnaire ainsi que son intensité, un modèle d'enroulement de la nappe tourbillonnaire est intégré dans Flap de sorte qu'aucune hypothèse supplémentaire n'est nécessaire. Ces modifications sont présentées et les améliorations des résultats ainsi obtenus sont clairement mis en évidence. La capacité du code à prédire le rayonnement acoustique d'un rotor pour différentes configurations de vol en utilisant un seul étalonnage est vérifier par comparaison avec la chaine de HMMAP de l'ONERA.

NB : Ce Tiré à part fait référence au Document d'Accompagnement de Publication DSNA14011

A PARAMETRIZED BVI NOISE PREDICTION CODE[†]

G. REBOUL[‡]
ONERA (DSNA/ACOU)
29 av. de la Division Leclerc
FR-92320 Châtillon

Abstract

The *Flap* code has been developed to predict blade vortex interaction noise at the early stage of development of a rotorcraft. For this purpose, the code needs to be fast and run with a small number of input data. This paper presents the last improvements that have been realized in the framework of the program CleanSky JTI, in which *Flap* is used to increase a database of noise radiated hemisphere. For each rotorcraft, reference computations are performed by DLR and CIRA using codes with a higher level of modelisation than *Flap* but also a higher computational time. These computations are then used to calibrate the *Flap* code which then will generate all the remaining necessary noise hemispheres. Consequently, the generalization of the wake model is necessary to allow good calibration. This is what, beside other improvements and after a short presentation of *Flap*, is presented in the beginning of the paper. However, the radial position of the vortex roll up and its intensity can not be easily calibrated; consequently, a roll up model is integrated in *Flap* so that no assumption has to be made. These modifications are presented and the resulting improvements of the results are clearly highlighted. The capacity of the code to predict the noise radiation on several flight configurations using only one calibration is check by comparison with the Onera comprehensive code HMMAP on a variation of the rotor angle of attack.

NOTATION

B	number of blade
c	airfoil chord, m
C_n	normal force coefficient
c_0	speed of sound, m/s
C_t	thrust coefficient
E	wake deviation angle
M	Mach number
R	rotor radius, m
r	blade element radial position, m
T	thrust, N
V_0	wind speed, m/s
α	aerodynamic angle of attack, °
α_s	rotor shaft angle of attack, °
Ω	rotational speed, rad/s
φ	azimuth, °
μ	advance ratio parameter
ν	rotor induced velocity, m/s
BVI	Blade Vortex Interaction
BPF	Blade Passing Frequency
HART	Higher harmonic control Aeroacoustic Rotor Test
SPL	Sound Pressure Level

INTRODUCTION

The *Flap* code has been developed to predict helicopter main rotor noise with emphasize on BVI (blade vortex interaction) noise at early stage of development. That means that the code needs to be fast in order to test a lot of configurations. It means also that the code needs to run with a small number of input data. A first presentation of the code has been made in [1]. Since this communication, a lot of improvements have been made in the framework of the program CleanSky JTI GRC7 (Green RotorCraft 7) [2].

As underlined in [1], the wake model represents the core of the problem since it determines how the blade and the vortices interact i-e, what are the angles of interactions and what is the intensity of the vortices during the interaction. This paper presents the improvements integrated in *Flap* concerning the wake model (based on the Beddoes model [3]) even if some improvements concerning other parts of the code have been made. For example, the possibility to use the lateral and longitudinal moments as input data to adjust the cyclic component of the pitch as it is already done with

[†] Presented at the Greener Aviation Conference, Brussels, Belgium, March 12-14, 2014
[‡] Corresponding author: Gabriel.Reboul@onera.fr

the thrust and the collective pitch angle, or the use of a Newton solver to efficiently solve this system of three equations. Consequently, the first part of summary of the major feature of the code is presented.

In the framework of the GRC7, the HELENA [4] code is used in order to determine the noise radiation. This code is based on a noise hemisphere database hemisphere database, with each hemisphere corresponding to a given rotorcraft and a specific flight condition. In this context, *Flap* is used to fill out this database. For each rotorcraft, references computations are performed by DLR (aerodynamic part) and CIRA (acoustic part) for three flight conditions using codes with a higher level of modelisation than *Flap*, but also a higher computational time. These computations are then used to calibrate the *Flap* code which then generates all the remaining necessary noise hemispheres. Consequently, the generalization of the wake model is necessary to allow good calibration. This is what, beside other improvements concerning the wake model, is presented in the second part of the report. However, some parameter can not be easily calibrated, such as the radial position of the vortex roll up and its intensity; consequently, a roll up model obtained from the Onera acoustic chain, HMMAP [5], is integrated in *Flap* so that no assumption has to be made. this modification is presented in the third part of the report. To check the capacity of the code to predict the noise radiation on several flight configurations using only one calibration, a comparison is performed with HMMAP with a variation of the rotor angle of attack.

1 *Flap* code main features

The main characteristics of the code are presented hereafter. The code is divided into four parts.

Trim module - The low frequency airloads are computed using quasi-steady linear aerodynamics including compressibility and three-dimensional corrections. Obviously, this aerodynamic model differs from the one used in the flight mechanics code and providing loads and moments as *Flap* inputs. Therefore the loads and the moments computed by *Flap* aerodynamics model need to be adjusted with those of the flight dynamics code. This adjustment is done by matching the mean thrust value with the input rotor thrust and the first harmonic with the moments. To solve efficiently this system of equation a Newton solver has been implemented.

Wake geometry module - The whole vorticity sheet geometry is computed using a semi-empirical model based on the model of Beddoes [3]. A roll-up model presented in [6] and already used in HMMAP [5] is used to determine the vortices position and strength. This feature of the code is detailed in the following.

BVI airloads module - The blade pressure fluctuations created by the BVI are computed using an analytical blade response function [7]. The main advantage of such function is that the shape of the blade doesn't need to be discretized since the airfoil is assimilated to a flat plate. The geometry of the interactions (angles and strength) is determined by the wake geometry module. These pressure fluctuations are added to the low frequency contribution computed in the trim module.

Noise radiation module - The Ffowcs-Williams and Hawkings solver PARIS [8] (also used in HMMAP) is used (in a compact chord approach) to determine the noise radiation from the blade pressure fluctuations.

2 Improvement and generalization of the Beddoes wake model

2.1 Wake geometry computation using a numerical integration

The Beddoes wake model [3] is based on an analytical integration of the expression of the induced velocity. Since the main objective is to improved the wake model, it is important not to be limited by expression of the induced velocity that has to be integrated analytically in order to obtain the position (X, Y, Z) of the vortex elements. Consequently, it is possible to solve this problem numerically since it consists on a simple convection problem with a time marching procedure. We denote the blade azimuth (time marching step) by the subscript i. These equations have to be solved for all the vortex segments, denoted by the subscript j. Finally, the system of equation to be solved is given by the equations 1 to 3.

$$X_{i,j} = \Delta t V_x + X_{i-1,j-1} \quad (1)$$

$$Y_{i,j} = Y_{i-1,j-1} \quad (2)$$

$$Z_{i,j} = \Delta t (V_z - \nu) + Z_{i-1,j-1} \quad (3)$$

with $j \leq i$. V_x and V_z are respectively the axial and vertical velocity and ν is the induced velocity which is a function of $X_{i,j}$ and $Y_{i,j}$.

This procedure is of course more time consuming than solving directly the analytical expression. To reduce the computational time, the wake position is solved with a relatively large azimuthal step of 10°. This discretization is of course not fine enough to accurately determine the position and the kinematic of the BVI. Consequently, the wake geometry is interpolated in a second step with much finer resolution, typically 0.3°.

2.2 Calibration capability

The Beddoes model is a semi-empirical model, which has of course a lot of limitation compared to a free wake code. This is especially true when dealing with BVI because a high precision is needed on the determination of the blade-vortex angles and distances. Consequently, one way to improve the result, is to generalize the model so that it can be modified and calibrated.

The classical Beddoes model gives the induced velocity ν under the rotor disk by :

$$\nu = \nu_0 \left(1 + Ex - Ey^3\right) \tag{4}$$

and outside the rotor disk by:

$$\nu = 2\nu_0 \left(1 - Ey^3\right) \tag{5}$$

where ν_0 is given by $\nu_0 = \lambda_0 \Omega R$. λ_0 is obtained by an iterative method to solve the equation 6 :

$$\lambda_0 = \frac{Ct}{2\sqrt{\mu_x^2 + (\lambda_0 - \mu_z)^2}} \tag{6}$$

Ct is the rotor thrust coefficient and E is the deviation angle of the rotor wake due to the rotor thrust:

$$E = \left| tan^{-1}\left(\frac{\mu_x}{(\lambda_0 - \mu_z)}\right)\right| \tag{7}$$

First, it is possible to introduced a lateral variation as proposed by Van der Wall [9] by adding the term $-2\mu_x y$ in the equations 4 and 5. Another modification is proposed by Van der Wall to respect the momentum theory on the mean value, it consist to add the term $\frac{8E}{15\pi}$. Finally, the induced velocity, as used in [1] is, under the rotor disk:

$$\nu = \nu_0 \left(1 + \frac{8E}{15\pi} - 2\mu_x y + Ex - Ey^3\right) \tag{8}$$

and outside the rotor disk by:

$$\nu = 2\nu_0 \left(1 + \frac{8E}{15\pi} - 2\mu_x y - Ey^3\right) \tag{9}$$

On this basis, one can add some coefficients as in equations 10 and 11 that will be used to calibrate the model.

Under the rotor disk :

$$\begin{aligned} \nu \;=\; & \nu_0 \left(K_0(1-\gamma_\zeta) + K_x Ex \right. \\ & \left. - 2K_y\mu_x y - K_\zeta E y^\zeta\right) \end{aligned} \tag{10}$$

and outside the rotor disk by:

$$\nu = 2\nu_0 \left(K_0(1-\gamma_\zeta) - 2K_y\mu_x y - K_\zeta E y^\zeta\right) \tag{11}$$

The coefficient γ_ζ is equal to $\frac{-8E}{15\pi}$ in 8 and 9 with $\zeta = 3$ and $K_\zeta = 1$. The modification of the parameter ζ will be treated in the section 2.3, and $\zeta = 3$ is supposed in the following application. We can remark that it is possible to increase the number of harmonics in these expressions. However, in equations 10 and 11, the Beddoes model is used as a basis making the calibration easier. By increasing the number of harmonics, the calibration will be much more complicated due to the absence of basis and the higher number of coefficients that have to be calibrated.

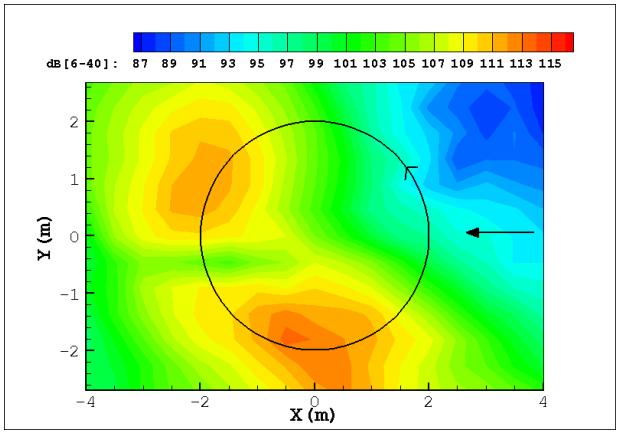

Figure 1: Noise footprint in dB [6-40 BPF]: measurement

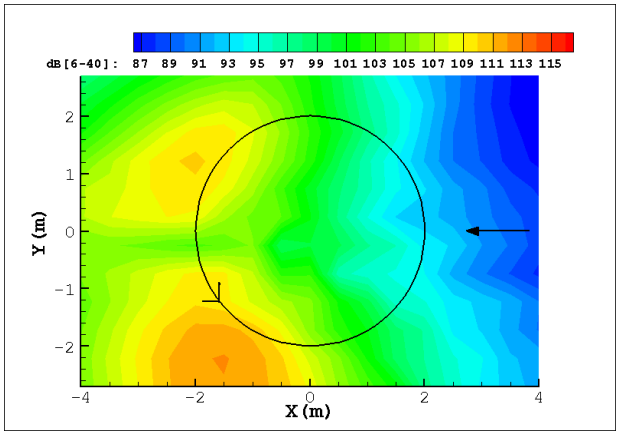

Figure 2: Noise footprint in dB [6-40 BPF]: *Flap* without calibration

Rotor radius, R	2 m
Blade chord, c	0.121 m
Root radius	0.44 m
Number of blades, B	4
Airfoil	NACA23012
Twist	-8°/R
Radius of zero twist	1.5 m
Wind speed, V_0	32.9 m/s
Speed of sound, c_0	341.7 m/s
Rotational speed, Ω	109 rad/s
Thrust, T	3300 N
Rotor shaft angle of attack, α_s	5.3° (4.5° with wind tunnel interference)

Table 1: Baseline test case of the HART II program

To illustrate this capacity, it is possible to use the baseline case of the HART II program [10], already used in [1]. The table 1 gives the main characteristics of this case. Figure 1 presents the noise footprint measured under the rotor disk. Without calibration, the *Flap* code gives the result presented in figure 2. On the retreating side the directivity is good with a small underestimation. On the advancing side, there is also a small underestimation, but the wake is too high resulting in too early interactions.

Then, if one modifies the coefficient as summarized in table 2, it is possible to improve the result as shown in figure 3. On the retreating side, the directivity is conserved but the level is a bit increase resulting in a good comparison with the experiment. On the advancing side, the interactions occur later because the wake is lower (increase of K_0). Consequently, the interaction are more efficient and a small overestimation is observed.

K_0	1.1
K_x	0.9
K_y	0.4
ζ	3
K_ζ	1

Table 2: Calibration coefficient corresponding to the result presented in figure 3

As a final comparison, figure 4 shows the result provided by the acoustic chain HMMAP [5] using more sophisticated but more time consuming methods. It appears that the calibration process produces a result close to the HMMAP prediction (tendency to overestimate the acoustic level on the advancing side). It has to be pointed out that the same flight mechanic input data have been used in both simulation. Consequently, it seems logical that simulations present similar tendencies.

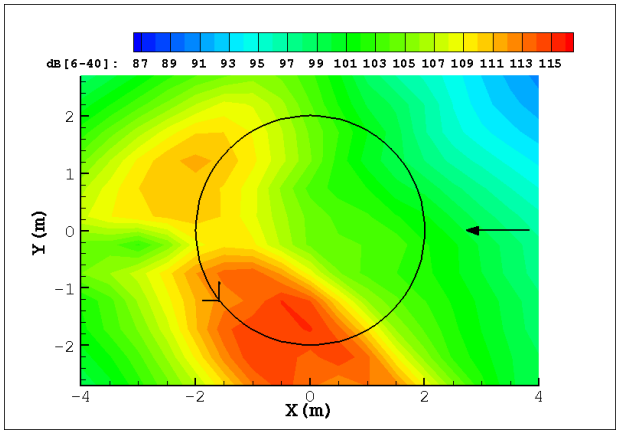

Figure 3: Noise footprint in dB [6-40 BPF]: *Flap* with calibration

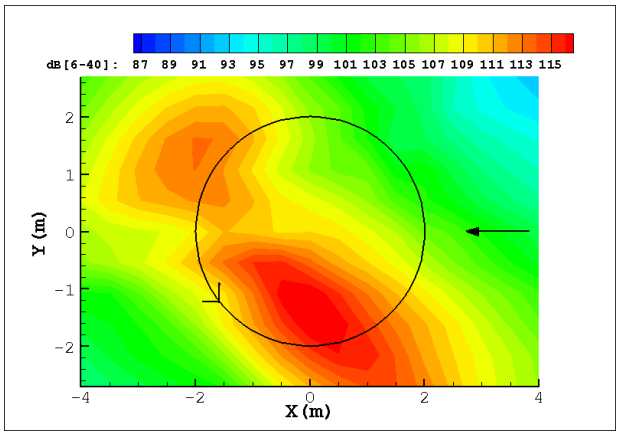

Figure 4: Noise footprint in dB [6-40 BPF]: HMMAP

2.3 Reduction of the rotor disk lifting part

One drawback of the Beddoes model is the absence of distinction between the central part and the rest of the disk. Since the lifting part of the blade does not extent in the rotor center, no induced velocity is generated in this part of the rotor disk. The same remark can be made close to the tip. Figure 5 presents an example of tip vortex position obtained by integration of equations 8 and 9 in a low speed descent flight. The wake stays low even when it goes under the rotor center, it should in fact go upward due to the absence of downwash. On the other hand, in figure 6, presenting the geometry for the same flight configuration obtained using a free wake code [5], one can clearly see the tip vortex going up when it passes under the center.

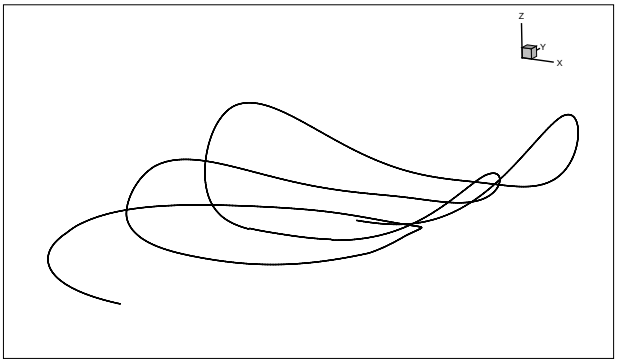

Figure 5: Baseline tip vortex position

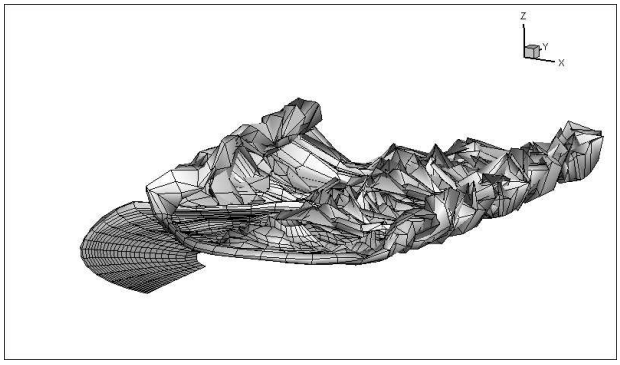

Figure 6: Wake position provided by a free wake code

This change in the geometry of the wake does not have a strong effect by it-self since the area of strong BVI is not involved. However, this leads to a change in the mean part of the expression changing consequently the height of the wake. To counter the absence of induced velocity in the center part of the disk, the downwash will be increased in the rest of the rotor plane, making the wake lower and changing the way the blades interact with the vortices. We can consider that the blade lift is approximately provided between 0.3R and 0.96R. The longitudinal and the lateral term of the induced velocity model are not affected contrary to the mean and the higher order lateral component. For the mean term, the integration on the reduced disk gives:

$$\int_0^{2\pi}\int_{0.3R}^{0.96R} r dr d\theta = \pi R^2(0.96^2 - 0.3^2) \qquad (12)$$

By identification with the area of the entire disk, a factor $0.96^2 - 0.3^2 = 1.2025$ has to be added. For the third order ($\zeta = 3$) lateral component:

$$\begin{aligned} & \int_0^{2\pi}\int_{0.3R}^{0.96R} K_\zeta E \left|y^3\right| r dr d\theta \qquad (13) \\ = \; & K_\zeta E \int_{0.3R}^{0.96R} \left|r^3\right| r dr \int_0^{2\pi} \left|sin^3\theta\right| \\ = \; & K_\zeta R^5 \frac{8}{15\pi}(0.96^5 - 0.3^5) \end{aligned}$$

A factor $\frac{8}{15\pi}(0.96^5 - 0.3^5) = 0.1659$ has to be introduced. One can remark that for a radial integration between 0 and R, we find the factor $\frac{8}{15\pi}$ already proposed by Van der Wall [9]. It is then possible to rewrite the induced velocity equations as:

- Under the rotor disk :

$$\begin{aligned} \nu \; = \; & \nu_0 \left(K_0(\chi_\zeta - \gamma_\zeta) + K_x E x \right. \qquad (14) \\ & \left. -2K_y\mu_x y - K_\zeta E y^\zeta\right) \end{aligned}$$

- Outside the rotor disk by:

$$\nu = 2\nu_0 \left(K_0(\chi_\zeta - \gamma_\zeta) - 2K_y\mu_x y - K_\zeta E y^\zeta\right) \qquad (15)$$

with $\chi_\zeta = 1.2025$. Table 3 gives the value of γ_ζ as a function of ζ.

ζ	γ_ζ
3	$-0.1659K_\zeta E$
4	$-0.1175K_\zeta E$
5	$-0.0876K_\zeta E$
6	$-0.0678K_\zeta E$
7	$-0.0539K_\zeta E$

Table 3: Calibration coefficient corresponding to the result presented in figure 3

In order to avoid an abrupt transition between the center of the rotor and the rest of the disk, a hyperbolic tangent function centered on 0.3R is used. The loss of induced velocity at the tip is not taken into account in the computation of the rotor wake geometry. Finally, the induced velocity integrated to provide the geometry is under the rotor disk :

$$\begin{aligned} \nu \; = \; & 0.5\nu_0 \left(tanh\left((r/R - 0.15)/0.05\right) + 1\right) \qquad (16) \\ & \times \left(K_0(\chi_\zeta - \gamma_\zeta) + K_x E x - 2K_y\mu_x y - K_\zeta E y^\zeta\right) \end{aligned}$$

and outside the rotor disk by:

$$\begin{aligned} \nu \; = \; & 0.5\nu_0 \left(tanh\left((r/R - 0.15)/0.05\right) + 1\right) \qquad (17) \\ & \times \left(K_0(\chi_\zeta - \gamma_\zeta) - 2K_y\mu_x y - K_\zeta E y^\zeta\right) \end{aligned}$$

In figure 7 one can clearly see the tip vortex going up when it passes through the rotor center.

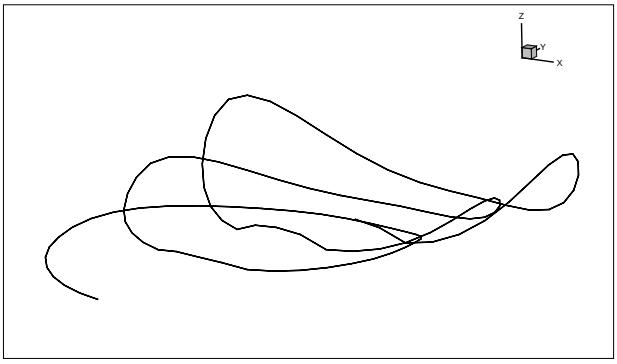

Figure 7: Tip vortex position with the improved Beddoes wake model

The noise footprint generated using this method is presented in figure 8. The result becomes close to the footprint obtained with calibration (cf. figure 3) since it implies a lower wake. However, the retreating side levels are underestimated and the levels on the advancing side are overestimated.

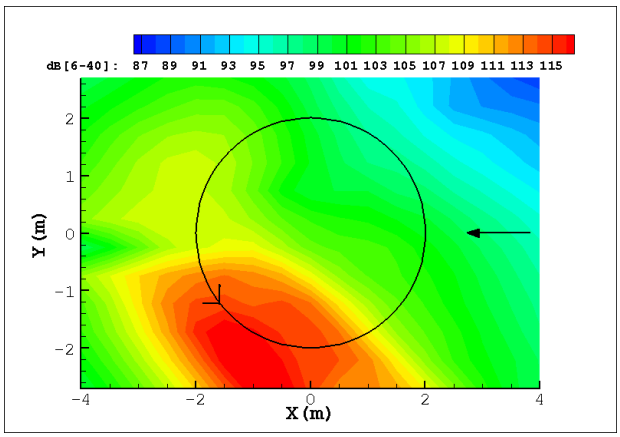

Figure 8: Noise footprint in dB [6-40 BPF]: *Flap* with an improved wake model

2.4 Low speed cases

The Beddoes wake model is only valid for a relatively high advance ratio. At low speed ($\mu \leq 0.05$ approximatively), a discontinuity is formed between the vortices that stays inside the rotor disk and the vortices that go outside the disk. In [11], Murakami et al. proposed a correction by introducing a factor depending of the advancing ratio. This factor writes $e^{-\xi\mu}$ and tends to zero as μ goes large. In order to increase the dependency in the advance ratio, the factor used here is $e^{-\xi\mu^2}$ with $\xi = 750$. Thus, the induced velocity outside the rotor disk becomes:

$$\begin{aligned} \nu &= 0.5\left(tanh\left(\left(r/R - 0.15\right)/0.05\right) + 1\right) \\ &\times \nu_0 \left(K_0(\chi_\zeta - \gamma_\zeta) - 2K_y\mu_x y - K_\zeta E y^\zeta\right) \\ &\times \left(2 - e^{-\xi\mu^2}\right) \end{aligned} \quad (18)$$

Figures 9(a) and 9(b) present a tip vortex geometry at $\mu = 0.012$ respectively without and with correction. This discontinuity is very important with the original model. When the correction is applied a smooth transition is obtained at the vicinity of the rotor. Nevertheless, minor discontinuities are visible in the far field.

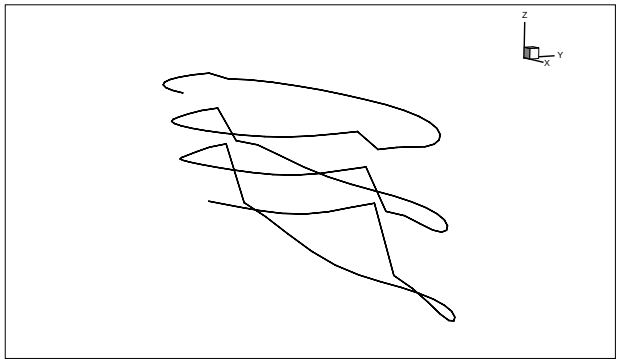

(a) Without correction

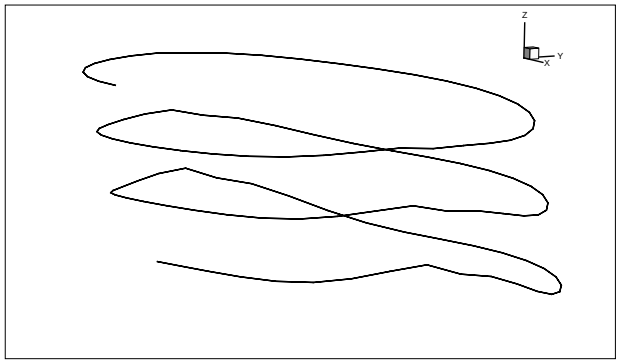

(b) With correction

Figure 9: Tip vortex trajectory at $\mu = 0.012$

3 Roll-up model incorporation

Another improvement realized in the *Flap* code concerns the introduction of a roll-up model. Using such a model, it is possible to remove two main hypothesis made initially. As a first hypothesis, we supposed that only the tip vortex was generated and that the radial position was equal to 0.98R. The second hypothesis concern the circulation of the vortex. In the initial version of *Flap*, the vortex circulation was equal to 85% of the maximum of circulation on the blade. The roll up model used here, named MENTHE [6], is the same as used in HMMAP. In MENTHE, the gradient of circulation on the blade is analysed in order to predict where the vortex will roll up and what will be it intensity. Consequently, there is no assumption on the number, the radial position and the intensity of vortices. However, this is costly in term of computational time since the whole vortex sheet has to be computed and not only one filament. To reduce the computational time and the necessary memory,

the roll up is computed before the interpolation (cf section 2.1) i-e with an azimuthal discretization of 10°. Finally, the interpolation is performed only on the rolled-up vortices.

Figure 10 is a view of the entire vortex sheet generated by a blade and the position of the roll up predicted by MENTHE (represented by the red thick line). In this case, only one vortex is generated but one can clearly see that its radial position evolves during the rotation.

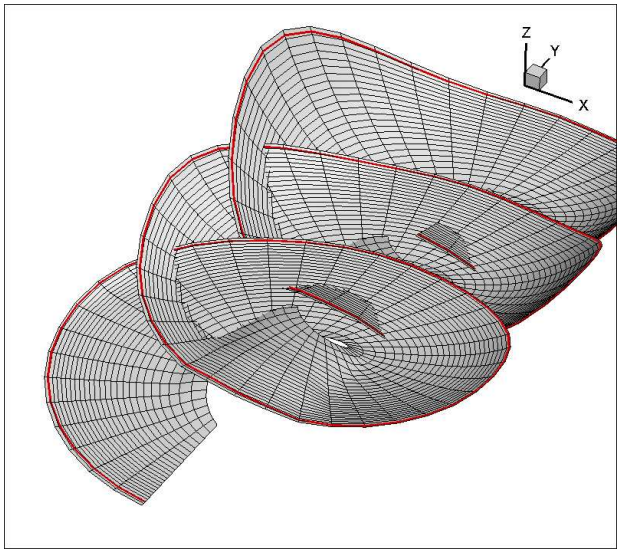

Figure 10: Vortex sheet position after three blade rotations (black meshes) and vortex roll-up position predicted by MENTHE (red line)

A last comparison can be made concerning this roll up process by looking at the evolution of the vortex circulation. Figure 11 presents the circulation for the initial *Flap* model, *Flap* with roll up model and HMMAP.

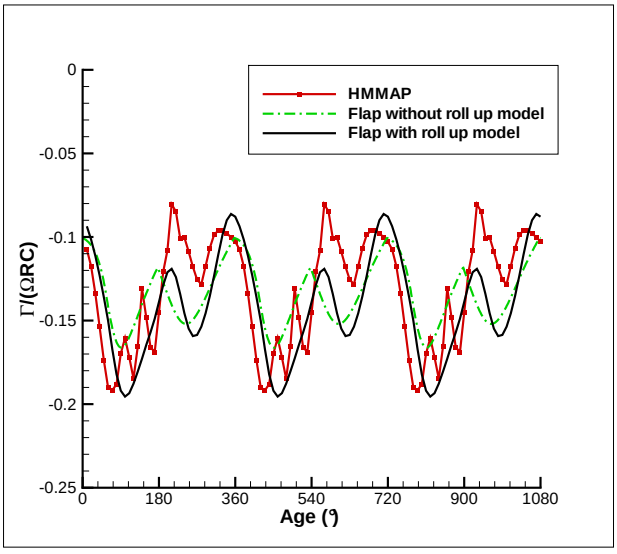

Figure 11: Vortex intensity as a function of age

The use of the roll-up model improves the results in terms on phase, but also in terms of amplitude without any calibration. The impact in terms of noises radiation is visible in figure 12. Once again, even without calibration, the results appear to be improved.

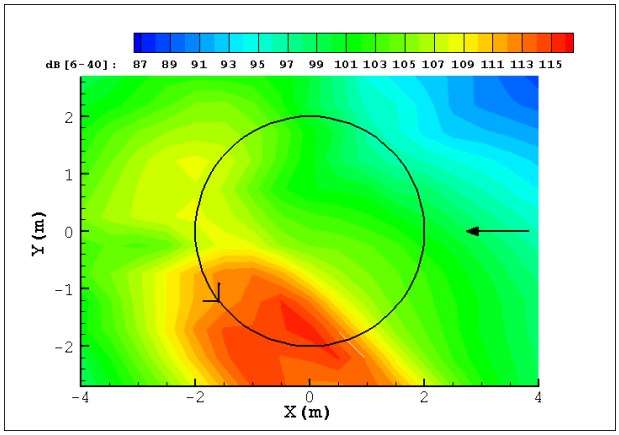

Figure 12: Noise footprint in dB [6-40 BPF]: *Flap* with an improved wake model and a roll up model

4 Illustration of calibration capability

In this section, the ability to compute the noise radiation on a complete flight envelop using *Flap* is studied. The rotor used is the same as the HART II rotor (40% mach scaled BO105 rotor). The comparaison is made with computation realized with HMMAP. The advance ratio is maintained constant and equal to 0.15 but the angle of attack varies from -8°, corresponding to a 10° climb, to 10° corresponding to a 8° approach. Figure 13 presents the evolution of the maximum noise level on a footprint under the rotor with and without calibration. The calibration is only performed for one flight configuration, the noisiest, at 4° of descent. Once the calibration coefficient are determined, all the other flight configuration are computed.

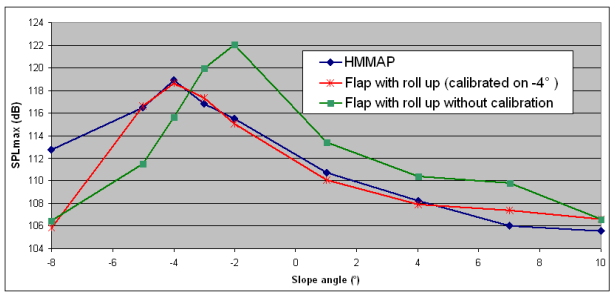

Figure 13: Maximum noise level radiated below the rotor as a function of the slope angle

Without calibration, the maximum noise level is shifted to higher descent angles and highly overestimated. Once the calibration is done, a clear improvement is observed on the BVI range from 4° to -5°. The effect of calibration is relatively weak outside this region. Finally a good agreement is obtained from 10° to -5° with a maximum discrepancy of 1.3 dB at 7°. The maximum noise level is predicted at the good configuration (-4°) and the reduction of the acoustic level with the reduction or the increase of the slope angle from -4° is well predicted. The only point showing a bad prediction is the last point at 8° of descent with 7dB of discrepancy.

Figures 14 to 20, illustrate the comparison between *Flap* with calibration and HMMAP by presenting the noise footprint under the rotor for different slope angle. The evolution of the directivity and the maximum noise level is well predicted by *Flap*. One can clearly see the maximum noise region going backward with the decrease of the slope angle. When the rotor angle of attack increases (and the slope angle decreases) the wake goes higher above the rotor and consequently the main interactions occur sooner during the rotation resulting in more backward acoustic directivities.

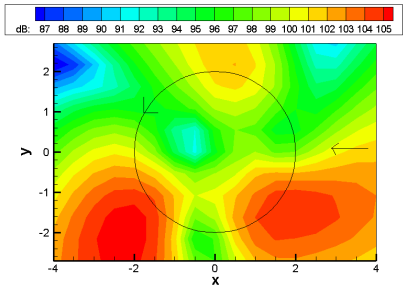

(a) HMMAP

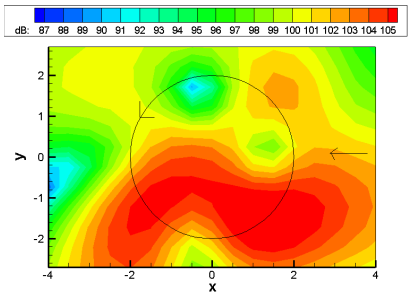

(b) *Flap*

Figure 14: Noise footprint in dB: 10° climb

On the 8° descent configuration, not only the levels are very different but also the directivity of the noise radiation. Even if both simulations are free of close BVI, the main acoustic radiation provided by HMMAP is due to blade pressure fluctuations caused by fluctuations of the induced velocity in the rear part of the rotor disc.

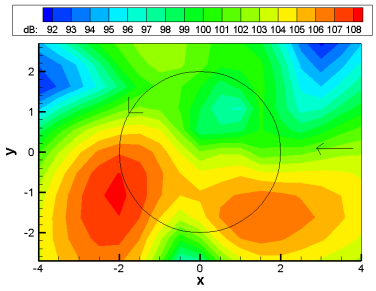

(a) HMMAP

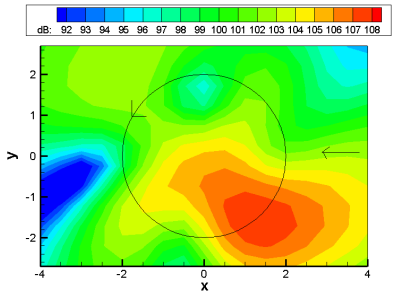

(b) *Flap*

Figure 15: Noise footprint in dB: 4° climb

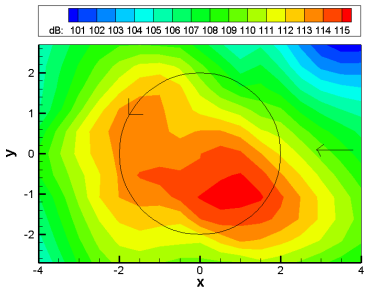

(a) HMMAP

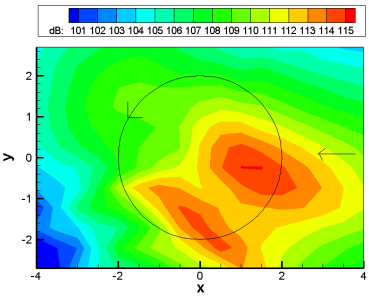

(b) *Flap*

Figure 16: Noise footprint in dB: 2° descent

The root vortices are not taken into account (in HMMAP and *Flap*) in the computation of close BVI but in HMMAP this vorticity will create fluctuations of induced velocity. This is possible because a coupling exists between the wake geometry and the induced velocity computations. Since it is not the case in *Flap*, this kind of induced velocity fluctuations are not predicted. The same phenomenon seems to occur during the climb with a smaller relative importance. However, one can note that, in

reality, these events are not physical since the rotor hub greatly reduces the root vortex. It can be conclude that using one point of calibration, the *Flap* code is able to extent the prediction to other flight configuration with a good level of accuracy.

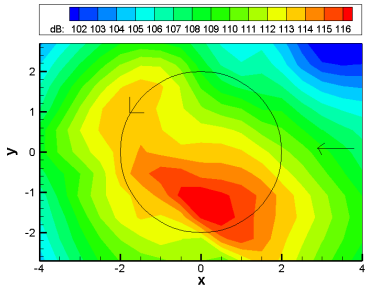

(a) HMMAP

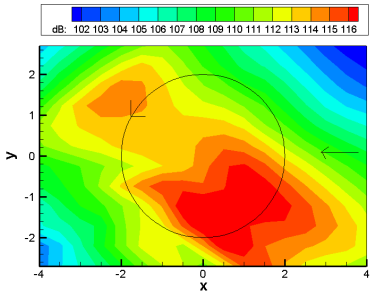

(b) *Flap*

Figure 17: Noise footprint in dB: 3° descent

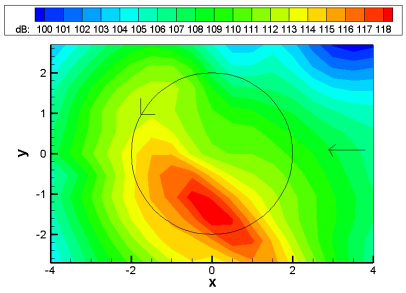

(a) HMMAP

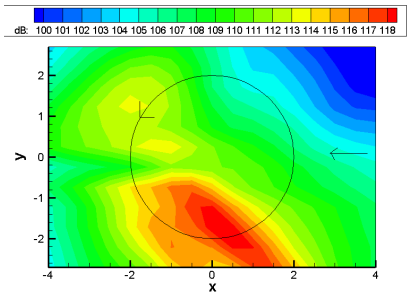

(b) *Flap*

Figure 18: Noise footprint in dB: 4° descent

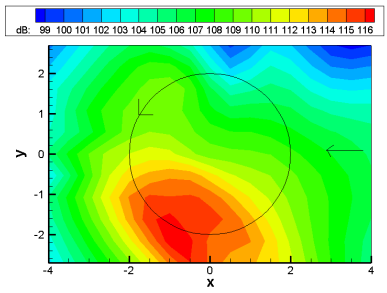

(a) HMMAP

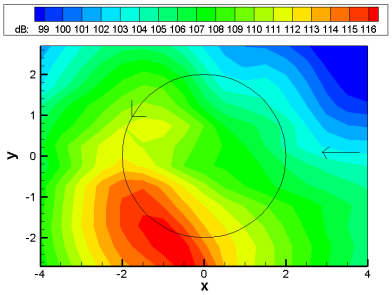

(b) *Flap*

Figure 19: Noise footprint in dB: 5° descent

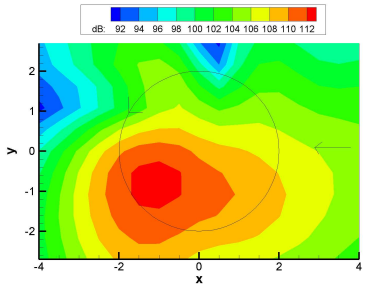

(a) HMMAP

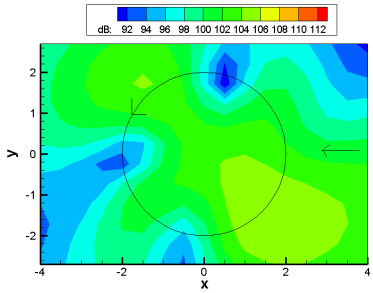

(b) *Flap*

Figure 20: Noise footprint in dB: 8° descent

CONCLUSION

The first part of this report presents recent developments realized in the code *Flap*. It is shown, how the Beddoes wake model can be improved by taking into account the fact that the central part of the rotor disk as well as its periphery is not lifting. The calibration of this wake model is made

possible by using four different coefficients and obtaining a generalization of the model. A numerical procedure is setup instead of an analytical integration of the induced velocity to obtain the wake geometry, so that there is no limitation in the induced velocity expression. Moreover, the limitation to large advance ratio of the Beddoes model is removed by using transition function depending on the square value of the advance ratio. Another major improvement presented in this report concerns the integration of a roll-up model. This model allows to determine how the vortex sheet is going to roll-up in term of position and intensity using the gradient of circulation along the blade. To highlight the benefits of the modifications, the HARTII baseline case is used and comparisons are made with the measurement and the Onera comprehensive code chain HMMAP. It clearly appears that these modifications of the code improve the results without increasing too much the computational time. Indeed, results become closer to the HMMAP results, which seems logical since both codes use the same trim condition as input.

The second part of the report deals with the calibration capacity of the code. A comparison with HMMAP is once again realized. It shows that if the calibration is done on the point of maximum noise level, the code *Flap* is able to predict with a good accuracy the noise radiation in terms of maximum noise level and directivity.

ACKNOWLEDGEMENT

This project is partly funded by the European Union in the framework of the Clean Sky program - Green Rotorcraft. This financial support is gratefully acknowledged. The author wants to acknowledge Joelle Bailly from the applied aerodynamic department at Onera for the aerodynamic computations in HMMAP.

References

[1] G. Reboul and A. Taghizad. Semi-analytical modelling of helicopter main rotor noise. In *Proceeding of the 38th European Rotorcraft Forum, Amsterdam, Netherland*, 2012.

[2] A. Antifora and F. Toulmay. CLEAN SKY - The GREEN ROTORCRAFT integrated technology demonstrator-state of play three years after kick-off. In *Proceedings of the 37th European Rotorcraft Forum, Ticino Park, Italy*, 2011.

[3] T. S. Beddoes. A wake model for high resolution airloads. In *Proceedings of the 2nd International Conference on Basic Rotorcraft Research, Triangle Park, USA*, 1985.

[4] M. Gervais, V. Gareton, A. Dummel, and R. Heger. Validation of EC130 and EC135 environmental impact assessment using HELENA. In *Proceedings of the 66th AHS Annual Forum, Phoenix, USA*, 2010.

[5] P. Beaumier and Y. Delrieux. Description and validation of the onera computational method for the prediction of blade-vortex interaction noise. In *Proceedings of the 29th Europeen Rotorcraft Forum*, 2003.

[6] G. Rahier and Y. Delrieux. Blade-vortex interaction noise prediction using a rotor wake roll-up model. *Journal of Aircraft*, 34 (4):522–530, 1997.

[7] L.T. Filotas. Vortex induced helicopter blade loads and noise. *Journal of Sound and Vibration*, 27(3):387–398, 1973.

[8] P. Spiegel and G. Rahier. Theoretical study and prediction of BVI noise including close interactions. In *Proceedings of the AHS Technical Specialists Meeting on Rotorcraft Acoustics and Fluid Dynamics, Philadelphia, USA*, 1991.

[9] B.G. van der Wall. The effect of HHC on the vortex convection in the wake of a helicopter rotor. *Aerospace Science and Technology*, 4:321–336, 2000.

[10] B.G. van der Wall, C.L. Burley, Y.H. Yu, K. Pengel, and P. Beaumier. The HART II test - measurement of helicopter rotor wakes. *Aerospace Science and Technology*, 8 (4), 2004.

[11] Y. Murakami, Y. Tanabe, S. Saito, and H. Sugawara. A new appreciation of prescribed wake models for cfd analysis in view of aeroacoustic applications. In *Proceeding of the 37th European Rotorcraft Forum, Vergiate and Gallarate, italy*, 2011.

ONERA
THE FRENCH AEROSPACE LAB

BP 72 - 29 avenue de la Division Leclerc - 92322 CHATILLON CEDEX - Tél. : +33 1 46 73 40 40 - Fax : +33 1 46 73 41 41

www.onera.fr